Respiratory Disease Prediction from Lung Sounds Using Reservoir Computing

Tushar Gupta, Vasundhara Damodaran, Jose Sanchez, Arindam Sanyal
School of Electrical, Computer and Energy Engineering, Arizona State University, Tempe, AZ, USA.
Email: tgupta39@asu.edu

2026 IEEE International Symposium on Circuits and Systems (ISCAS) | 979-8-3315-7769-8/26/$31.00 ©2026 IEEE | DOI: 10.1109/ISCAS66217.2026.11562147

***Abstract*—Respiratory diseases are among the leading causes of mortality worldwide, including in the United States. Respiratory sounds provide critical insight into pulmonary health, as they are directly influenced by airflow dynamics, changes in lung tissue, and the presence of secretions within the tracheobronchial tree [1]. In this work, we present an artificial intelligence (AI)–based approach for predicting respiratory diseases from lung sounds, integrated into a wearable platform for on-device monitoring. Using the ICBHI 2017 Respiratory Sound Database [2], our method demonstrates strong performance in both binary classification (Healthy vs. Unhealthy) and multiclass classification (six respiratory diseases). The proposed solution employs an analog reservoir computer (RC) fabricated in a 28 nm CMOS process, achieving energy-efficient operation with a consumption of only 12.9nJ per prediction for multiclass and 7.4nJ per prediction for binary class, while reaching 91% accuracy for binary classification and 89% accuracy for multiclass classification.**

***Index Terms*—Reservoir-computing, respiratory sounds, machine learning, analog circuits, switched-capacitor**

I. Introduction

Respiratory diseases such as chronic obstructive pulmonary disease (COPD) is among the leading causes of mortality worldwide, responsible for over 3 million deaths annually according to the World Health Organization (WHO) [3]. These conditions remain widely underdiagnosed and poorly managed, imposing a significant burden on healthcare systems. The COVID-19 pandemic further exacerbated this challenge, introducing additional respiratory complications such as wheezing and stridor, and underscoring the need for early and accurate detection of respiratory disorders [4]. Advances in digital health technologies, including digital stethoscopes, have transformed respiratory monitoring by enabling continuous, noninvasive, and objective assessment of lung health. Lung sounds carry critical diagnostic information—adventitious sounds such as crackles and wheezes are key indicators of pulmonary dysfunction [2], [5]. However, traditional auscultation remains subjective and dependent on clinical expertise, often leading to variability and missed early signs of disease. Computational Lung Sound Analysis (CLSA) addresses these limitations by integrating digital sound acquisition with signal processing and machine learning to automatically detect, classify, and interpret abnormal respiratory sounds [6]. This computational framework enhances diagnostic consistency and supports scalable, automated monitoring in telemedicine and wearable platforms.

Within CLSA, two main classification tasks are typically explored: (i) detection of adventitious lung sounds and (ii) respiratory disease classification (RDC). This work focuses on the latter, performing both binary (healthy vs. unhealthy) and multiclass classification across pathological categories using a reservoir computing (RC)–based approach evaluated on the ICBHI 2017 dataset [2].

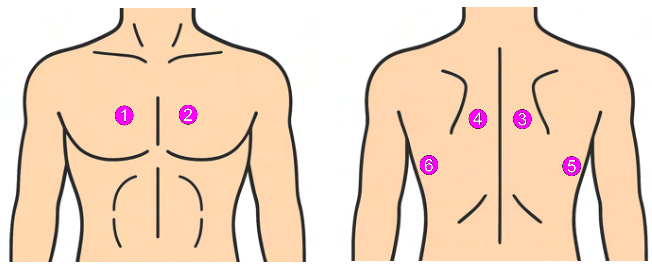

Fig. 1. Chest locations for recording of respiratory sounds [2]

Several studies have utilized the ICBHI 2017 dataset for respiratory disease classification (RDC). Dang et al. [7] achieved F1-scores of 96.6% and 93.22% for binary and multiclass tasks using a CNN with Log-Mel features. Chua and Cheng [8] proposed a lightweight multi-head attention model achieving an ICBHI score of 59.2% on a four-class task, while Ordas et al. [9] employed a CNN with a variational convolutional autoencoder to mitigate class imbalance, reaching a 99.3% F1-score for three classes. Despite these advances, deploying such models on wearable devices remains constrained by high computational and energy demands. Existing approaches—such as low-bit precision and in-/near-memory computing—offer partial relief but still incur energy costs of hundreds of nJ to few µJ per inference [10]–[14]. To address this limitation, we introduce an analog reservoir computing (RC) framework that harnesses inherent analog non-idealities to simplify circuit design and drastically reduce energy consumption. The remainder of this paper is organized as follows: Section II describes the dataset, Section III details the RC architecture, Section IV presents 28 nm test-chip results, and Section V concludes the paper.

II. The ICBHI 2017 Dataset

The International Conference on Biomedical and Health Informatics (ICBHI) 2017 dataset [2] comprises 920 annotated audio samples from 126 subjects, covering both healthy and seven respiratory disease categories: Pneumonia, Bronchiectasis, COPD, Upper Respiratory Tract Infection (URTI), Lower Respiratory Tract Infection (LRTI), Bronchiolitis, and

Asthma. Recordings were collected using multiple stethoscopes (AKGC417L, Meditron, Litt3200, and LittC2SE), with durations ranging from 10–90 s and sampling rates between 4 kHz and 44.1 kHz. Each recording contains several breathing cycles annotated with start and end times, as well as the presence or absence of crackles and wheezes. In total, the dataset includes 6898 respiratory cycles, consisting of 3642 normal, 1864 crackle, 886 wheeze, and 506 mixed (crackles + wheezes) cycles. The average cycle duration is 2.7 s, ranging from 0.2 s to 16 s.

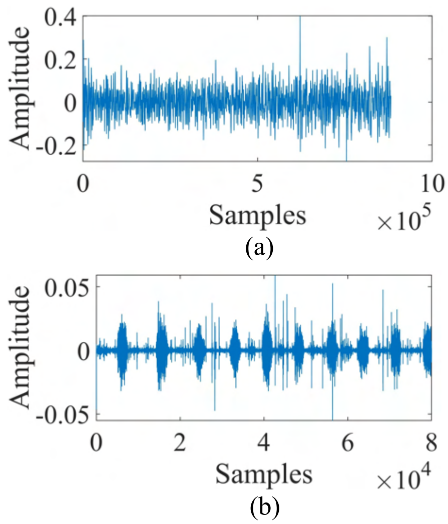

Fig. 2. Plot of Lung Sound a) before pre-processing and b) after pre-processing and noise filtering

During preprocessing, each lung sound segment was re-sampled to 4 kHz for uniformity. A 4th-order Butterworth band-pass filter (100–2000 Hz) was then applied to remove background noise and retain the frequency range relevant to respiratory sounds as shown in Fig. 2. The Asthma and LRTI classes were excluded due to their limited sample counts, yielding a more balanced dataset for multiclass classification.

This work addresses the Respiratory Disease Classification (RDC) task, consisting of two sub-tasks. The first is a binary classification that distinguishes healthy and unhealthy samples, where the unhealthy class combines five disease categories (excluding Asthma and LRTI). The second is a multiclass classification that differentiates between healthy and five disease categories. The dataset was divided by the ICBHI challenge into 60% for training and 40% for testing. Both sets are composed with different patients (i.e. non-overlapping). The train set was further divided into 80% train and 20% validation set with no overlapping between the patients.

III. Proposed Architecture

A. Overview of RC circuits

RC is a bio-inspired framework derived from Recurrent Neural Networks (RNNs), originating from two independent models in early 2000s: the echo state network (ESN) [15] and the liquid state machine (LSM) [16]. Related approaches, including the back-propagation decorrelation (BPDC) algorithm [17] and corticostriatal models of the prefrontal cortex [18], were later unified under the RC paradigm by Verstraeten et al. [19]. An RC network consists of a reservoir and a readout layer. The reservoir, formed by randomly connected neurons, produces complex transient responses to inputs that serve as high-dimensional states. These states are linearly combined by the readout layer to generate outputs. During training, the reservoir weights remain fixed, and only the readout layer is trained by learning algorithms [20] which leads to low computation, and simple hardware realization. With inherent temporal memory, RC efficiently handles sequential and time-varying signals and has been implemented across several hardware domains, including optical, neuromorphic, and quantum systems. Early optical RCs were demonstrated in [21], [22], followed by photonic implementations [23]–[25], FPGA-based realizations [26], and memristive reservoirs for pattern classification [27]. Analog silicon RCs have been reported in [28]–[31], though many rely on large capacitors to emulate biological time constants or require analog delay calibration, both of which limit energy efficiency. Our prior work [31] introduced an on-chip analog RC using time-multiplexing to create multiple virtual neurons from a single physical neuron, eliminating large capacitors and calibration. However, it used continuous-time circuits, which are inefficient for biomedical signals due to static power dissipation. The present work advances beyond [31] by employing a switched-capacitor RC architecture that achieves a $5\times$ reduction in energy consumption and enables complete on-chip neuron integration.

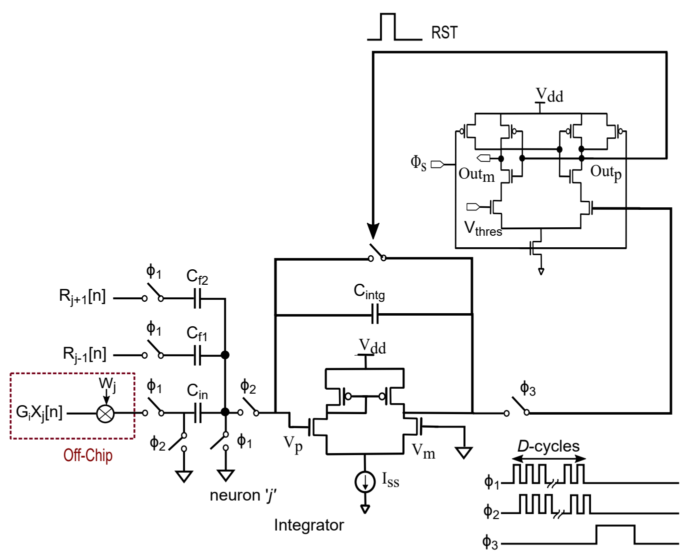

Fig. 3. Schematic of the Reservoir layer Neuron

B. Circuit design

Fig. 3 shows the schematic of the reservoir layer neuron. Output of the RC with N reservoir neurons can be mathematically expressed as

$$\vec{R}_k[n] = H\left(G_i\vec{W} \times \vec{X}[n] + G_f\vec{W}_r \times \vec{R}_k[n-1]\right) \qquad (1)$$

where $R_k[n]$ is output of the k-th reservoir neuron at the n-th time sample, $\vec{X}$ is the input with D samples, $\vec{W}$ is $N \times D$ input weight matrix, $\vec{W}$, $\vec{W_r}$ is $N \times N$ inter-connection weight matrix for the reservoir layer, $H(\cdot)$ is nonlinear activation for the reservoir neuron, G_i is input scaling factor and G_f is feedback gain. Weights in both the input and reservoir layers are generally initialized from random distributions, while only the output layer undergoes training. Elements in the input and reservoir weight matrices are restricted to 0/1, reducing computation complexities. At the input layer, RC receives an input vector $\vec{X}$ with D features, multiplies it with input weight matrix. Multiplication of the input samples with $\vec{W}$ is carried off-chip which facilitates testing the chip with different input sample sizes D. This output is then send to the reservoir which performs non-linear projection with N neurons. The interconnect matrix $\vec{W_r}$ is sparsely populated and provides the reservoir layer with the memory, enabling the RC to display high-dimensional characteristics despite having a relatively small number of neurons. Since RC uses non-linearity for input projection, the otherwise undesired non-linearities in analog circuits become useful attributes and relaxes the circuit design allowing it to be low power and small area. The recurrent neural network behavior is realized in circuit using a leaky integrator with a low-gain amplifier (≈ 25). Matrix multiplications are performed in charge-domain using switched-capacitors. The integrator is reset if its output exceeds a threshold voltage. Each reservoir neuron is connected to two immediately neighbouring neurons. The reservoir employs lateral inhibition, such that all three neurons within a cluster reset when any one neuron triggers a reset. This mechanism, inspired by the human retina, enhances transient detection. The feedback gain (G_f) and input scaling factor (G_i) are set by the ratios of sampling capacitors C_{in}, C_{f1}, and C_{f2} to the integration capacitor C_{intg}. The nonlinearity in reservoir originates from multiple sources: (a) amplifier nonlinearity during slew mode, (b) integrator reset behavior, and (c) charge injection in the switching network. Unlike conventional analog designs that demand precise matching or high linearity, the proposed RC neurons are compact and mismatch-tolerant, as these non-idealities are naturally absorbed into the reservoir kernel. Key parameters - including neuron count (N), feedback gain, input scaling, and interconnect sparsity - were optimized using software based RC simulations. The RC layer output feeds a two-layer artificial neural network (ANN). The number of hidden neurons was determined through hyperparameter optimization using the software RC model.

Before analysis with the RC, time-domain feature extraction is performed on the lung sound samples. Seven time-domain features are computed to capture key statistical properties of the waveform: mean and standard deviation of peaks, mean and standard deviation of peak-to-peak distances, number of peaks, and mean and standard deviation of the lung sound segment. Only time-domain features are used, rather than a combination of time and frequency features, to reduce energy consumption. As reported in [32], combining frequency and time-domain features yields comparable classification performance to time-domain features alone while consuming significantly more energy. Software simulations were performed to determine the optimal network configuration. The reservoir uses $N = 20$ neurons, and the ANN comprises a hidden layer of 60 neurons and an output layer of 1 neuron. Additional simulations were conducted to optimize input scaling (G_i) and feedback gain (G_f), ensuring efficient RC performance. As shown in Fig. 4, software model for RDC task of multiclass achieved a maximum accuracy of around 90% for G_i=0.2 and G_f=0.1.

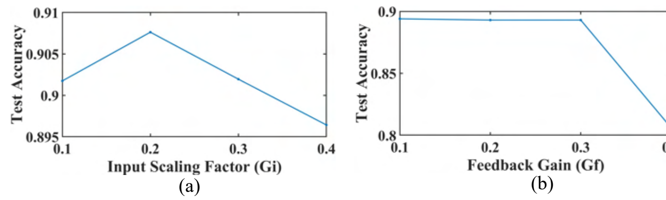

Fig. 4. For 6-class RDC a) Plot of Test Accuracy vs G_i and b) Plot of Test Accuracy vs G_f

IV. Evaluation

A test chip was fabricated in a 28 nm CMOS process, with the layout and die micrograph shown in Fig. 5. The chip occupies a area of 1.64mm×1.04mm and integrates 30 on-chip neurons. Operating from a 0.9 V supply at 31.25 kHz, the measured energy consumption for the multiclass RDC task is 0.1 nJ for input, 0.1 nJ for reservoir, and 12.7 nJ ANN layer, resulting in a total energy of 12.9 nJ. For the binary class RDC task, the corresponding energy consumption is 0.1 nJ for input, 0.1 nJ for reservoir, and 7.2 nJ for ANN, yielding a total of 7.4 nJ. Input samples are applied to the test chip using National Instruments Data Acquisition (DAQ) hardware, and the chip outputs are captured via a logic analyzer, as illustrated in Fig. 6.

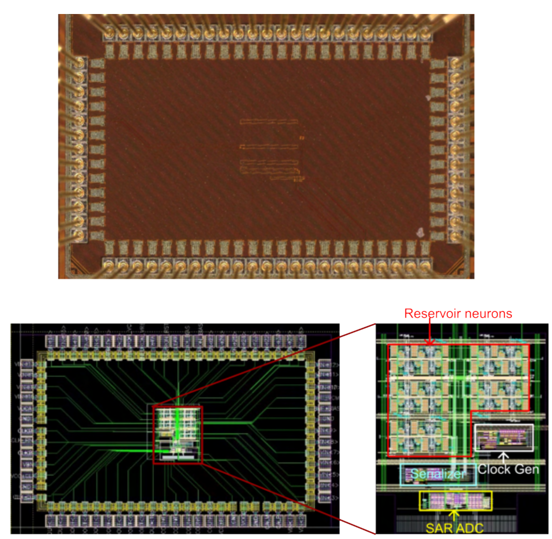

Fig. 5. Layout view and die microphotograph.

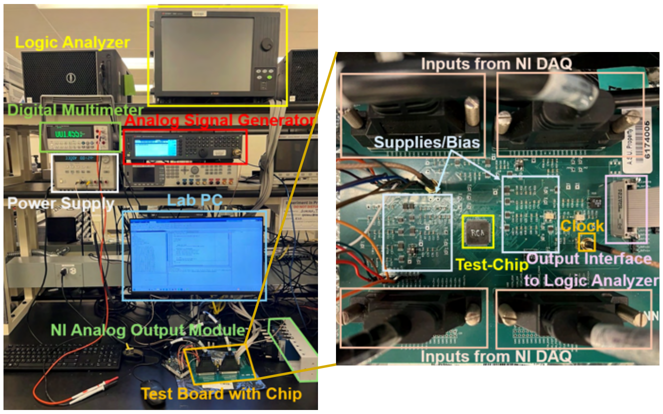

Fig. 6. Picture of the test setup and test board with the chip and equipment interfaces.

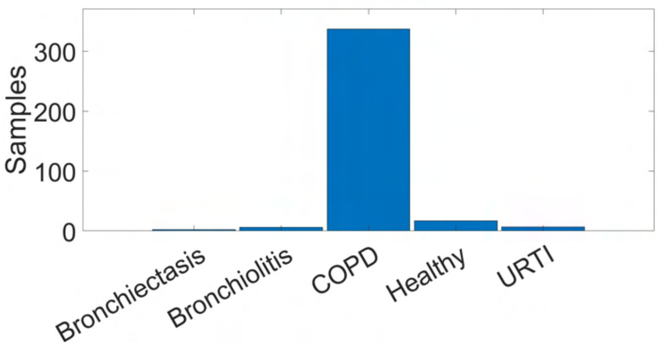

Fig. 7. Distribution of diseases in test set

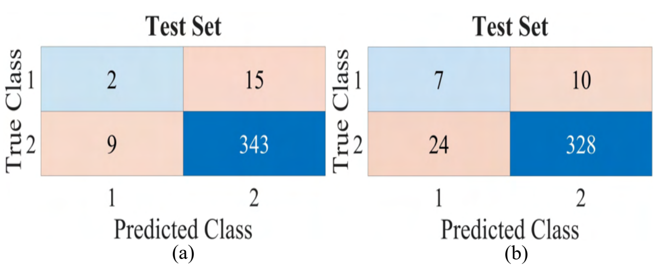

Fig. 8. 2-Class (1 – Healthy, 2 – Unhealthy) RDC Confusion Matrix for (a) Software Model (b) 28nm Test-Chip.

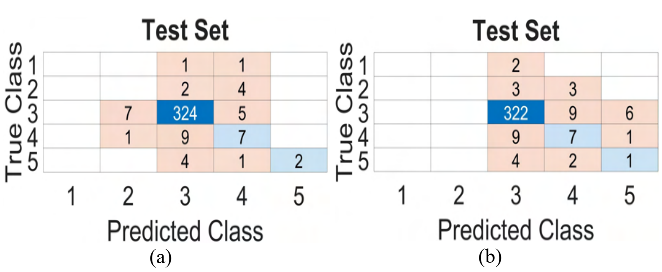

Fig. 9. 5-Class (1 – Bronchiectasis, 2 – Bronchiolitis, 3 – COPD, 4 – Healthy, and 5 – URTI) RDC Confusion Matrix for (a) Software Model (b) 28nm Test-Chip.

The test-set confusion matrices for the binary and multiclass RDC tasks are shown in Fig. 8 and Fig. 9, respectively. In the binary task, Class 1 represents healthy and Class 2 unhealthy subjects. The multiclass task includes six training categories: (1) Bronchiectasis, (2) Bronchiolitis, (3) COPD, (4) Healthy, (5) URTI, and (6) Pneumonia. As shown in Fig. 7, the test set contains only five classes, with Class 6 (Pneumonia) appearing exclusively in the training data.

Table I compares the proposed method with state-of-the-art approaches. CNN-based models [33], [34] achieve F1-scores of 81% and 88%, respectively, but are compute-intensive and unsuitable for low-power deployment. ResNet50 with Log-Mel features [35] and Log-Mel/MFCC feature based models in [36] require computationally intensive preprocessing. TriSpectraKAN [37] combines spectral features with the Kolmogorov–Arnold Network (KAN), leading to high hardware cost and latency [38]. The VGGish–BiGRU model [39] relies on a pretrained CNN, increasing model complexity and overfitting risk on small datasets. In contrast, the proposed switched-capacitor RC is compact, energy-efficient, and achieves comparable F1 performance for binary and multiclass classification while being optimized for on-device, low-power respiratory disease classification.

V. Conclusion

This work presents an analog switched-capacitor RC architecture for respiratory disease classification using lung sounds. The proposed design achieves enhanced energy efficiency compared to prior implementations by leveraging the low-power operation of switched-capacitor circuits. Owing to its scalable architecture and relaxed analog design requirements, the system can be readily ported to advanced technology nodes for further reductions in energy and area. The demonstrated results highlight the potential of the proposed energy-efficient neuromorphic circuit for integration into next-generation edge and wearable health-monitoring devices.

TABLE I
Comparison with the State-of-the-Art

	Design	Classes	F1-Score	Energy/Inf.
Zhang et al. [33]	Software (CNN)	6	81.0%	-
A.Roy et al. [37]	Software (TriSpectraKAN)	6	97.0%	-
Y.Choi et al. [36]	Software (LACM Attention)	6	92.3%	-
TNyugen et al. [35]	Software (ResNet50)	2	80.7%	-
K.N. Lal et al. [39]	Software (BiGRU)	2	95.0%	-
D.Perna et al. [34]	Software (CNN)	2	88.0%	-
This Work	**ASIC (28nm test-chip)**	**5***	**89.4%**	**12.9nJ**
		2	**91.3%**	**7.4nJ**

* test set consists of only 5 classes

Acknowledgment

This work is supported by SRC through task #3160.033.and Alphacore Inc. under DoE grant number DE-SC0022923.

References

[1] J. Earis and B. Cheetham, "Current methods used for computerized respiratory sound analysis," *European Respiratory Review*, vol. 10, pp. 586–590, 01 2000.

[2] B. M. Rocha, D. Filos, L. Mendes, I. Vogiatzis, E. Perantoni, E. Kaimakamis, P. Natsiavas, A. Oliveira, C. Jácome, A. Marques, R. P. Paiva, I. Chouvarda, P. Carvalho, and N. Maglaveras, "A respiratory sound database for the development of automated classification," in *Precision Medicine Powered by pHealth and Connected Health*, N. Maglaveras, I. Chouvarda, and P. de Carvalho, Eds. Singapore: Springer Singapore, 2018, pp. 33–37.

[3] "Chronic obstructive pulmonary disease (COPD) — who.int," https://www.who.int/news-room/fact-sheets/detail/chronic-obstructive-pulmonary-disease-(copd), 2024.

[4] M. Barbosa, M. Morais-Almeida, C. Sousa, and J. Bousquet, "The "big five" lung diseases in covid-19 pandemic – a google trends analysis," *Pulmonology*, vol. 27, no. 1, pp. 71–72, 2021, pMID: 32636165.

[5] M. Sarkar, I. Madabhavi, N. Niranjan, and M. Dogra, "Auscultation of the respiratory system," *Annals of thoracic medicine*, vol. 10, pp. 158–168, 07 2015.

[6] R. X. A. Pramono, S. A. Bowyer, and E. Rodríguez-Villegas, "Automatic adventitious respiratory sound analysis: A systematic review," *PLoS ONE*, vol. 12, 2017. [Online]. Available: https://api.semanticscholar.org/CorpusID:9994261

[7] M. N. N. Dang, N. D. Nghiem, T. S. Pham, N. V. Hoang, T. M. Tran, and T. T. K. Nguyen, " Respiratory Disease Classification Using IPMix and Custom Deep Learning Architectures ," in *2025 IEEE/ACIS 23rd International Conference on Software Engineering Research, Management and Applications (SERA)*. Los Alamitos, CA, USA: IEEE Computer Society, May 2025, pp. 567–572.

[8] Y.-W. Chua and Y.-C. Cheng, "Towards enhanced classification of abnormal lung sound in multi-breath: A light weight multi-label and multi-head attention classification method," 2024. [Online]. Available: https://arxiv.org/abs/2407.10828

[9] M. T. García-Ordás, J. A. Benítez-Andrades, I. García-Rodríguez, C. Benavides, and H. Alaiz-Moretón, "Detecting respiratory pathologies using convolutional neural networks and variational autoencoders for unbalancing data," *Sensors*, vol. 20, no. 4, 2020.

[10] K. H. Lee and N. Verma, "A low-power processor with configurable embedded machine-learning accelerators for high-order and adaptive analysis of medical-sensor signals," *IEEE Journal of Solid-State Circuits*, vol. 48, no. 7, pp. 1625–1637, 2013.

[11] S. M. Abubakar, M. R. Khan, W. Saadeh, and M. A. B. Altaf, "A wearable auto-patient adaptive ECG processor for shockable cardiac arrhythmia," in *IEEE Asian Solid-State Circuits Conference (A-SSCC)*, 2018, pp. 267–268.

[12] S. Yin, M. Kim, D. Kadetotad, Y. Liu, C. Bae, S. J. Kim, Y. Cao, and J.-s. Seo, "A 1.06-μ W Smart ECG Processor in 65-nm CMOS for Real-Time Biometric Authentication and Personal Cardiac Monitoring," *IEEE Journal of Solid-State Circuits*, vol. 54, no. 8, pp. 2316–2326, 2019.

[13] J. Liu, Z. Zhu, Y. Zhou, N. Wang, G. Dai, Q. Liu, J. Xiao, Y. Xie, Z. Zhong, H. Liu *et al.*, "BioAIP: A Reconfigurable Biomedical AI Processor with Adaptive Learning for Versatile Intelligent Health Monitoring," in *IEEE International Solid-State Circuits Conference (ISSCC)*, vol. 64, 2021, pp. 62–64.

[14] F. C. Bauer, D. R. Muir, and G. Indiveri, "Real-time ultra-low power ECG anomaly detection using an event-driven neuromorphic processor," *IEEE Transactions on Biomedical Circuits and Systems*, vol. 13, no. 6, pp. 1575–1582, 2019.

[15] H. Jaeger, "The" echo state" approach to analysing and training recurrent neural networks-with an erratum note'," *Bonn, Germany: German National Research Center for Information Technology GMD Technical Report*, vol. 148, 01 2001.

[16] W. Maass, T. Natschläger, and H. Markram, "Real-time computing without stable states: a new framework for neural computation based on perturbations," *Neural Comput*, vol. 14, no. 11, pp. 2531–2560, Nov. 2002.

[17] J. Steil, "Backpropagation-decorrelation: online recurrent learning with o(n) complexity," in *2004 IEEE International Joint Conference on Neural Networks (IEEE Cat. No.04CH37541)*, vol. 2, 2004, pp. 843–848 vol.2.

[18] P. F. Dominey, "Complex sensory-motor sequence learning based on recurrent state representation and reinforcement learning," *Biological Cybernetics*, vol. 73, no. 3, pp. 265–274, Aug 1995.

[19] D. Verstraeten, B. Schrauwen, M. D'Haene, and D. Stroobandt, "An experimental unification of reservoir computing methods," *Neural Netw*, vol. 20, no. 3, pp. 391–403, Apr. 2007.

[20] H. Zhang and D. Vargas, "A survey on reservoir computing and its interdisciplinary applications beyond traditional machine learning," *IEEE Access*, vol. PP, pp. 1–1, 01 2023.

[21] K. Vandoorne, W. Dierckx, B. Schrauwen, D. Verstraeten, R. Baets, P. Bienstman, and J. V. Campenhout, "Toward optical signal processing using photonic reservoir computing," *Opt. Express*, vol. 16, no. 15, pp. 11 182–11 192, Jul 2008.

[22] K. Vandoorne, P. Mechet, T. Van Vaerenbergh, M. Fiers, G. Morthier, D. Verstraeten, B. Schrauwen, J. Dambre, and P. Bienstman, "Experimental demonstration of reservoir computing on a silicon photonics chip," *Nature Communications*, vol. 5, no. 1, p. 3541, Mar 2014.

[23] A. Katumba, J. Heyvaert, B. Schneider, S. Uvin, J. Dambre, and P. Bienstman, "Low-loss photonic reservoir computing with multimode photonic integrated circuits," *Scientific Reports*, vol. 8, no. 1, p. 2653, Feb 2018.

[24] C. Sugano, K. Kanno, and A. Uchida, "Reservoir computing using multiple lasers with feedback on a photonic integrated circuit," *IEEE Journal of Selected Topics in Quantum Electronics*, vol. 26, no. 1, pp. 1–9, 2020.

[25] K. Takano, C. Sugano, M. Inubushi, K. Yoshimura, S. Sunada, K. Kanno, and A. Uchida, "Compact reservoir computing with a photonic integrated circuit," *Opt. Express*, vol. 26, no. 22, pp. 29 424–29 439, Oct 2018.

[26] Verstraeten, David and Schrauwen, Benjamin and Stroobandt, Dirk, "Reservoir Computing with Stochastic Bitstream Neurons," in *Proceedings of the 16th Annual ProRISC Workshop*, 2005, pp. 454–459.

[27] M. S. Kulkarni and C. Teuscher, "Memristor-based reservoir computing," in *Proceedings of the 2012 IEEE/ACM International Symposium on Nanoscale Architectures*, ser. NANOARCH '12. New York, NY, USA: Association for Computing Machinery, 2012, p. 226–232. [Online]. Available: https://doi.org/10.1145/2765491.2765531

[28] F. Bauer, D. Muir, and G. Indiveri, "Real-time ultra-low power ecg anomaly detection using an event-driven neuromorphic processor," *IEEE Transactions on Biomedical Circuits and Systems*, vol. PP, pp. 1–1, 11 2019.

[29] K. Bai and Y. Yi, "Dfr: An energy-efficient analog delay feedback reservoir computing system for brain-inspired computing," *J. Emerg. Technol. Comput. Syst.*, vol. 14, no. 4, Dec. 2018. [Online]. Available: https://doi.org/10.1145/3264659

[30] Y. Chen, E. Yao, and A. Basu, "A 128-channel extreme learning machine-based neural decoder for brain machine interfaces," *IEEE Transactions on Biomedical Circuits and Systems*, vol. 10, no. 3, pp. 679–692, 2016.

[31] S. T. Chandrasekaran, I. Banerjee, and A. Sanyal, "7.5nj/inference cmos echo state network for coronary heart disease prediction," in *ESSDERC 2021 - IEEE 51st European Solid-State Device Research Conference (ESSDERC)*, 2021, pp. 103–106.

[32] S. P. Bhanushali, S. Sadasivuni, I. Banerjee, and A. Sanyal, "Digital machine learning circuit for real-time stress detection from wearable ECG sensor," in *IEEE 63rd International Midwest Symposium on Circuits and Systems (MWSCAS)*, 2020, pp. 978–981.

[33] P. Zhang, A. Swaminathan, and A. Uddin, "Pulmonary disease detection and classification in patient respiratory audio files using long short-term memory neural networks," *Frontiers in Medicine*, vol. 10, 11 2023.

[34] D. Perna, "Convolutional neural networks learning from respiratory data," in *2018 IEEE International Conference on Bioinformatics and Biomedicine (BIBM)*, 2018, pp. 2109–2113.

[35] T. Nguyen and F. Pernkopf, "Lung sound classification using co-tuning and stochastic normalization," *IEEE Transactions on Biomedical Engineering*, vol. 69, no. 9, pp. 2872–2882, 2022.

[36] Y. Choi and H. Lee, "Interpretation of lung disease classification with light attention connected module," *Biomedical signal processing and control*, vol. 84, p. 104695, 03 2023.

[37] A. Roy, B. Gyanchandani, A. Oza, and A. Singh, "Trispectrakan: a novel approach for copd detection via lung sound analysis," *Scientific Reports*, vol. 15, no. 1, p. 6296, Feb 2025.

[38] V. D. Tran, T. X. H. Le, T. D. Tran, H. L. Pham, V. T. D. Le, T. H. Vu, V. T. Nguyen, and Y. Nakashima, "Exploring the limitations of kolmogorov-arnold networks in classification: Insights to software training and hardware implementation," 2024. [Online]. Available: https://arxiv.org/abs/2407.17790

[39] K. N. Lal, "A lung sound recognition model to diagnoses the respiratory diseases by using transfer learning," *Multimedia Tools and Applications*, vol. 82, no. 23, pp. 36 615–36 631, Sep 2023.